Toward Seven-Band Coherent WDM System Covering T to U Bands: Predictions of Transmission and BER Performance

Arwa A. Moosa[1,2], Raad Sami Fyath [3]

Authors affiliations:

1) Department of Laser and Optoelectronics Engineering, College of Engineering, Al-Nahrain University, Baghdad, Iraq.
2) Department of Networks Engineering, College of Engineering, Al- Iraqia University Baghdad, Iraq.
eng.arwa.amir@gmail.com
arwa.amir@al-iraqia.edu.iq

3) Department of Computer Engineering College of Engineering, Al-Nahrain University, Baghdad, Iraq.
rsfyath@yahoo.com

Abstract

This paper discusses the development of a seven-band coherent wavelength-division multiplexing (WDM) system covering the T to U systems, aiming to enhance the capacity and system efficiency. Seven multiband systems (C+L, S+C+L, S+C+L+U, E+S+C+L, E+S+C+L+U, O+E+S+C+L+U, and T+O+E+S+C+L+U) are designed with 40 GBaud symbol rate, 50 GHz channel spacing, and dual-polarization (DP)-16QAM signaling. The analysis adopted the enhanced Gaussian noise model, considering the amplified spontaneous emission of inline optical amplifiers and nonlinear interference (NLI) from fiber nonlinear optics, including Kerr effect and stimulated Raman scattering (SRS) which it implemented using Matlab (Ver. 2020b) program. The results show that the optimal powers are -4, -5, -5, -4.5, -3.5, -6, and -4.5 dBm for the seven WDM systems, respectively. Further, with a fiber span length of 100 km, the C+L system has the longest transmission reach of 20 span. However, using S+C+L+U system gives the highest bit rate-distance product of 1619 Tbps.km. The O+E+S+C+L+U and T+O+E+S+C+L+U systems are designed with 50 km-span length to reduce the effect of NLI caused by the large numbers of channels (1060 and 1200, respectively).

Keywords: Seven-band WDM, UWB-WDM, Enhanced Gaussian noise model, Optical communication bands.

التوجه نحو نظام WDM متماسك ذي سبعة نطاقات يغطي نطاقات T إلى U: تنبؤات الإرسال وأداء BER

اروى عامر موسى ، رعد سامي فياض

الخلاصة:

تناقش هذه الورقة تطوير نظام تعدد الإرسال بتقسيم الطول الموجي المتماسك ذي النطاقات السبعة (WDM) الذي يغطي أنظمة T إلى U، بهدف تعزيز قدرة وكفاءة النظام. سبعة أنظمة متعددة النطاقات (C+L، S+C+L، S+C+L+U، E+S+C+L، E+S+C+L+U، O+E+S+C+L, وتم تصميم U و T+O+E+S+C+L+U) بمعدل رمز ٤٠ جيجا بايت، وتباعد القنوات ٥٠ جيجا هرتز، وإشارة الاستقطاب المزدوج (DP)-16QAM. اعتمد التحليل نموذج الضوضاء الغوسية المعزز، مع الأخذ في الاعتبار الانبعاث التلقائي المضخم للمكبرات الضوئية المضمنة والتداخل غير الخطي (NLI) من البصريات غير الخطية للألياف، بما في ذلك تأثير كير وتشتت رامان المحفز (SRS) والتي تم تنفيذها باستخدام برنامج Matlab (الإصدار ٢٠٢٠ب). أظهرت النتائج أن القوى المثلى هي ٤-، ٥-، ٥-، ٤.٥-، ٣.٥-، ٦-، و ٤.٥- ديسيبل ميلي واط لأنظمة WDM السبعة، على التوالي. علاوة على ذلك، مع طول نطاق ألياف يبلغ ١٠٠ كم، يتمتع نظام C+L بأطول مدى للإرسال يصل إلى ٢٠ نطاقًا. ومع ذلك، فإن استخدام نظام S+C+L+U يعطي أعلى معدل بت للمسافة يبلغ ١٦١٩ تيرابت في الثانية.كم. تم تصميم أنظمة O+E+S+C+L+U وT+O+E+S+C+L+U بطول ٥٠ كم لتقليل تأثير NLI الناتج عن الأعداد الكبيرة من القنوات (١٠٦٠ و١٢٠٠ على التوالي).

1. Introduction

Optical communication systems face a continuous data traffic growth to support advanced multimedia and internet of things (IoT) applications [1] and [2]. Several studies have been suggested to increase the transmission capacity of wavelength-division multiplexing (WDM) [3] system by decreasing the channel spacing and increasing the number of channels; up to 281 channels have been reported in C band of 4.5 THz bandwidth [4]. Novel approaches have been suggested to use ultra-wideband (UWB) WDM technique beyond the conventional C band as listed in Table (A) of Appendix A. A WDM system of C+L band with more than 10 THz bandwidth has been widely proposed in the literature because L and C bands have almost the same fiber parameters values [5]. In addition, both bands may share the same photonic devices such as optical amplifiers [6]. Further, scientific and engineering research has propagated toward S+C+L system where the three bands have the lowest attenuation window in standard single-mode fiber (SMF), which is considered as a very achievable way for expanding transmission capacity [7], [8], [9], [10], [11], and [12]. Covering S to U band has been also investigated to obtain both higher capacity and spectral efficiency as done in [13] due to its lower band attenuation values. Further, because of the development of ITU-T G.652D SMF, which provides a low water peak absorption, the use of O+E+S+C+L band is possible for transmission, which increases the bandwidth more than six times in comparison to the C-band transmission [14] and [15]. Table (A) summarizes the main concepts of the scanned literature related to UWB-WDM systems; The main conclusions drawn from this table are

I.   The use of more bands to implement the WDM system attracts increasing interest although more research is needed to design UWB equipment.

II.   Most research focused on the three-UWB WDM, S+C+L (S2L), system. It is expected that going to insert more bands will give a higher data transmission rate especially for low transmission distance.

III.   The used method to estimate the optimal power was based on optimizing a single-band transmission by sweeping the power, then reoptimizing the system by entering another single band. This method is very complex and takes a relatively long time for high -number of channel system.

Consider the seven-band (T2U) UWB-WDM system, whose optical spectrum extends from T to U bands, as shown in Figure (1) with parameters listed in Table (1).
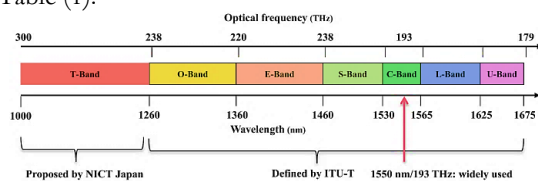
Table (1): Spectral range of the bands used in future WDM systems.

Band	Spectrum range (nm)	Center wavelength (nm)	Bandwidth (THz)
T (Thousand Band)	1000 -1260	1130.0	62.0
O (Original Band)	1260 -1360	1310.0	17.4
E (Extended Band)	1360-1460	1410.0	15.1
S (Short Band)	1460-1530	1495.0	09.4
C (Convention al Band)	1530-1565	1547.5	04.4
L (Long Band)	1565-1625	1595.0	07.0
U (Ultra-Long Band)	1625-1675	1650.0	05.5

This WDM system is a promising candidate for the next generation of optical communication networks [16]. The UWB-WDM is considered the most advantageous manner to enlarge the capacity without replacing the existing fiber infrastructure, which offers dramatic efficiencies in the cost and delay of system deployment [17]. This paper investigates the transmission performance of seven UWB-WDM systems incorporating DP-16QAM modulation format, 40 GBaud symbol rate, and 50 GHz frequency channel. The systems are C+L (C2L), S+C+L (S2L), S+C+L+U (S2U), E+S+C+L (E2L), E+S+C+L+U (E2U), O+E+S+C+L+U (O2U), and T+O+E+S+C+L+U (T2U). The investigation is based on enhanced Gaussian noise (EGN) model which takes into account the nonlinear interference (NLI) due to nonlinear fiber optics and amplificated spontaneous emission (ASE) noise, beside the amount of power transfer from high- to low- frequency channel caused by stimulated Raman scattering (SRS) effect.

The key contributions of this work as related to the seven UWB-WDM systems are as follows

I.   Investigating the linear and nonlinear spectral characteristics of the SMF when used as the transmission link for WDM systems.

II.   Studying the effect of fiber nonlinearity on the shape of the received optical signal spectrum by investigating the individual contributions of self-phase modulation (SPM) and cross-phase modulation (XPM) to NLI.

III.   Recording both signal quality as a function of signal received power and Bit error BER performance as a function of transmission distance.

IV.   Estimating the optimal power required to minimize the BER for a given link length and taking the highest-edge channel of UWB-WDM system as a reference.

Figure (1): Spectral regions of the seven bands used in next UWB-WDM systems [16].

V. Recording the maximum transmission reach (MTR) as a function of channel lunch power.

The rest of the paper is organized as follows. Section II presents a summary of the estimated main SMF spectral parameters including attenuation, dispersion, and nonlinear optics. The UWB-WDM system configuration is described in Section III. The mathematical frame work is described in Section IV where the main used equations are taken from published references. Section V contains simulation results related to NLI spectra, optimal channel power, and MTR. Section VI states briefly challenges facing the implementation of UWB-WDM systems. Section VII gives a summary of the main conclusions drawn from this study.

2. Primary Concepts of Multiband WDM Fiber Communication System

To transmit an UWB-WDM system over a SMF, the spectra of several linear and nonlinear fiber effects should be considered [18]. In this work, comprehensive estimation of fiber frequency-dependent parameters is performed including the linear parameters (such as attenuation and dispersion) and nonlinear parameters (such as Kerr-related nonlinear parameter and Raman gain slope). For space limitation, only a summary of the results is reported in this section.

The attenuation of a SMF has an effect on signal transmission quality and it is estimated here over the UWB spectrum (1000 to 1700 nm) as shown in Figure (2). Fiber loss (attenuation) comes mainly from scattering loss, infrared radiation (IR), and Hydroxide (OH^-) absorption [19]. Therefore, low water-peak absorption fiber, ITU-T G-652.D, is preferred to be used [20] because it reduces the effect of peaks absorption as shown in Figure (2). To simplify the calculations during system simulation, the attenuation coefficients are estimated at the center wavelengths of each band and assumed to be constant through the whole band. This assumption is justified here since the variation of fiber parameters over a single band is relatively small. The estimated attenuation coefficients at the center wavelengths of T, O, E, S, C, L, U bands (1130, 1310, 1410, 1495, 1547.5, 1595, and 1650 nm) are 0.5, 0.29, 0.24, 0.20, 0.17, 0.18, 0.24 dB/km, respectively.
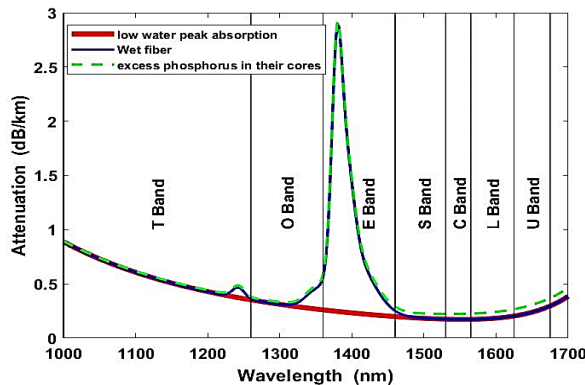
Figure (2): Estimated attenuation coefficient of SMF as a function of wavelength.

The spectral characteristics of total chromatic dispersion D and its components, marital D_M and waveguide D_W, are also estimated as given in Figure (3). The calculations use the wavelength-dependance of both core and cladding reflective indices, n and n_c, as described by Sellmeier Equation. Accordingly [21] and [22]

$$D(\lambda) = D_W(\lambda) + D_M(\lambda) \quad\quad …..(1.a)$$
$$D_M(\lambda) = -(\lambda/c)(d^2\lambda/dn^2) \quad\quad …..(1.b)$$
$$D_W(\lambda) = -(n_c\,\Delta/c\,\lambda)\,(Vd^2(Vb)/\,dV^2) \quad (1.c)$$

where Δ is the relative index difference, λ is the wavelength, V is the V-number (normalized frequency), c is the speed of light in vacuum, and b is the normalized propagation constant and λ is the wavelength. Further, dy/dx and d^2y/dx^2, respectively, for the first and second derivatives.

From Figure (3), the estimated chromatic dispersion coefficients at the center frequencies of T, O, E, S, C, L, and U bands are -20.04, 0, 7.31, 13.70, 17.00, 19.73, 22.99 ps/nm/km, respectively. The dispersion slope parameter S can be estimated when D is known at a reference wavelength λ_{ref} by

$$S \equiv \frac{dD}{d\lambda} \cong \frac{D(\lambda) - D(\lambda_{ref})}{\lambda - \lambda_{ref}} \quad\quad ……(2)$$

The S parameter is useful for the operation of digital signal processing (DSP) unit implemented in each channel receiver to compensate the grope-velocity dispersion D at the channel wavelength.
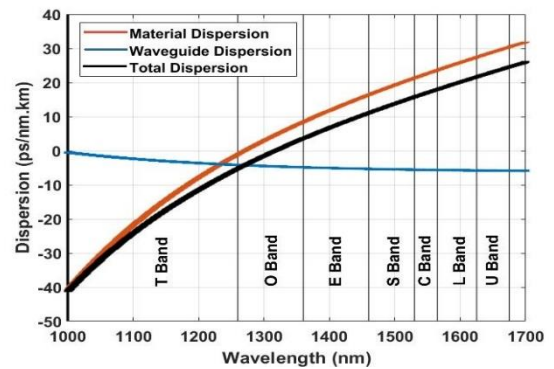
Figure (3): Chromatic dispersion coefficients of SMF as a function of wavelength.

Besides these two linear effects, nonlinear fiber optics should be taken into account due to the high light intensity, that caused by the large number of channels in the UWB-WDM system that transfer at the same time through the SMF. The fiber core refractive index n is modified according to Kerr effect by $n = n_0 + n_2 I$, where n_0 is low-intensity core refractive index and n_2 is the nonlinear refractive index coefficient of the core material [23]. This effect can be expressed by fiber Kerr nonlinear parameter γ which is estimated as a function of wavelength from 1000 to 1700 nm as shown in Figure (4). The parameter γ is defined as $\gamma(\lambda) \equiv 2\pi n_2/\lambda A_{eff}$ [24], and its calculated after estimating the spectral of fiber effective area characteristics A_{eff} as in [25]. Figure (4)

shows that the fiber nonlinear parameter γ decreases with wavelength and it is equal to 1.81, 1.56, 1.45, 1.38, 1.30, 1.28, and 1.24 1/W/km at the center wavelengths of the bands, respectively.
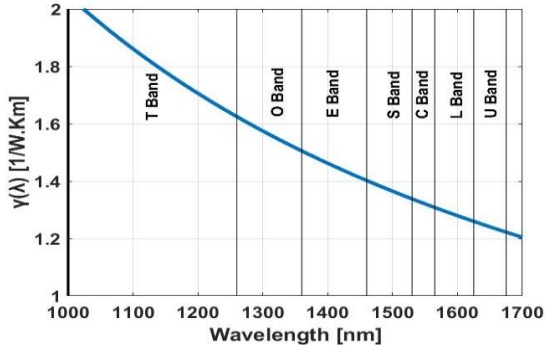
Figure (4): Nonlinear parameter γ of SMF over T2U UWB range.

The effect of stimulated Raman scattering (SRS) is also considered in this work, which causes a power transfer ΔP from high-to low-frequency channels. This influences the distribution of signal power of the ith channel (channel under observation) according to the expression reported in [39] for S+C+L system and generalized in this work by Eqn. 3 for any multiband-WDM system

$$\Delta P(z) = \sum_{q_{lower}}^{i} 4.3 C_r L_{eff} (P_{tot})_{lower} (B_{tot})_{lower} \quad \dots\dots(3)$$

where q_{lower} is the maximum number of low-frequency neighboring channels with respect to the ith channel which are involved in SRS effect, $(P_{tot})_{lower}$ is the total channel launch power of the lower-band frequency, $(B_{tot})_{lower}$ is the total bandwidth of lower-band frequency, C_r is the Raman gain slope coefficient, and $L_{eff} = (1 - \exp(\alpha L))/\alpha$ is the effective length with L is the fiber length and α is the attenuation. Note that the C_r for each band can also be considered as

$$C_{r@\lambda} = C_{r\,@ref} \times \lambda_{ref}/\lambda \quad \dots\dots(4)$$

From Equation (4), C_r is equal to 0.037, 0.032, 0.029, 0.028, 0.027, 0.026 and 0.025 ((1/W)/km)/THz at the center wavelength of each band.

3. UWD-WDM System Configuration

Figure (5) shows a simplified schematic diagram of the T2U UWB-WDM fiber communication system. The main parameters of each band used in the calculations are listed in Table (2). A 1 THz-band guard is inserted between successive bands to ensure efficient band demultiplexing at the receiver side. Further, only 7 THz portion of T band (246-239 THz) is used here since this wideband is not expected to be fully occupied by WDM technology in the near future due to the lake off efficient photonics and optical devices. Table (2) indicates that the used bandwidths of the T, O, E, S, C, L, and U bands are 7, 16, 14 ,8, 4, 6 and 5, respectively. Assuming a WDM system operates with 40 GBaud symbol rate R_s and 50 GHz

channel spacing Δf , and DP-16QAM signaling, then the number of channels carried by each band are 140, 320, 280, 160, 80, 120, and 100, respectively. Thus 1200 channels may be carried by the T2U system. Table (2) also gives the values of fiber parameters $\alpha, D, S,$ and γ estimated at the center frequency of the used bandwidth of each band.

At the WDM transmitter side, a bank of 1200 continues-wave (CW) lasers are modulated using DP-16QAM signaling and then multiplexed and transmitted through loss-compensated N_s-span link. Each span consists of a SMF section of type IUT-TG-652 followed by an UWB optical amplification scheme (OAS) to compensate the span loss as shown in Figure (6). The OAS consists of three cascaded stages where first and last stage are implemented using band demultiplexer (to separate the bands) and band multiplexer (to combine the amplified band signals), respectively. The intermediate stage uses seven optical amplifiers (OAs) configured in parallel where each OA is responsible for fiber span loss compensation of a given band. The gain of each band OA is decibel is computed as $G\,(dB) = \alpha\,(dB/km) \times L_s\,(km)$, where α is fiber loss estimated at the center frequency of the band and L_s represents the span length.
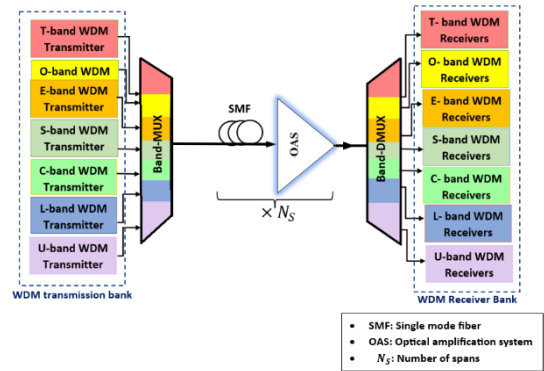
Figure (5): T2U UWB-WDM system.
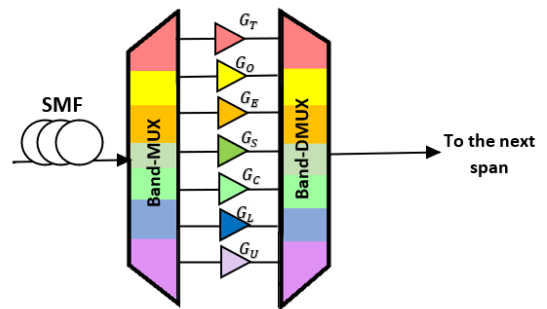
Figure (6): Signal span configuration which consists of SMF section follows by an optical amplification system (OSA). The ith band optical amplifier is labeled with the symbol Gi which denotes its optical gain.

A simplified block diagram of a single-band WDM transmitter is illustrated in Figure (7. a). The CW laser bank transmits N channels, from ch1 to chN, where N depends on the used band spectral bandwidth B and channel spacing Δf ($N = B/\Delta f$). Each optical channel carrier is modulated using the corresponding

channel data by a DP-16QAM optical modulator. The modulated signals are multiplexed using a channel band multiplexer resulting a band WDM signal. At the end of the fiber, the corresponding band WDM receiver operates as illustrated in Figure (7. b). The received band WDM signal is demultiplexed by a channel demultiplexer and then a channel data recovery is achieved by a coherent channel detection. The optical DP-16QAM channel transmitter and receiver are illustrated in the block diagram of Figures (8. a &b), respectively. The UWB-WDM system configuration adopted in this work are depicted in figures (5-7) which are by the authors themselves.

Figure (8. a) shows a single-channel transmitter of the DP-QAM system, The binary data are applied to a binary-to-symbols mapper which produces two groups of symbols (X-symbols and Y-symbols). At the same time, a $45°$-polarized CW laser field is split into two orthogonal polarization components. These two components are modulated by X-and Y- channel data using two independent in-phase quadrature (IQ) modulators. The two orthogonal polarized modulated signals X-QAM and Y-QAM are then combined using a polarization beam combiner to generate the DP-QAM channel signal. The channel receiver uses a DP-QAM digital coherent detective system. At the WDM receiver side, each received channel signal is split into two orthogonally polarized components by a polarization beam splitter. Two 90° optical hybrids are used to combine the received signal with the CW local laser field component, in each polarization state. The $45^°$-polarization state of the local laser ensures equal-power polarized components. These two 90° hybrid devices act as a 2×4 quadrature optical hybrid. It combines two input signals (CW reference signal and received signal) and generates four output optical signals with a 90° phase shift. The output signal is then detected by two identical photodiodes and after filtering the signal is applied to a dual-polarization DSP unit for further signal improvement, such as compensating the chromatic dispersion for the channel under observation.
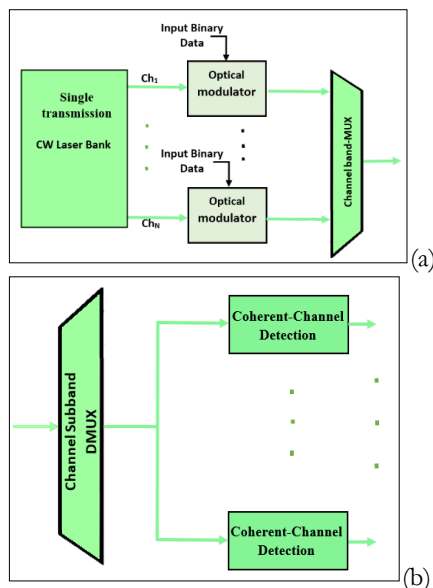
Figure (7): A single-band WDM (a) transmitter and (b) receiver.
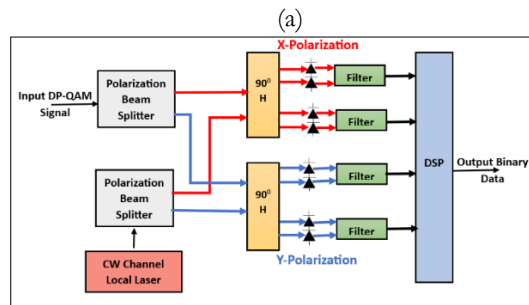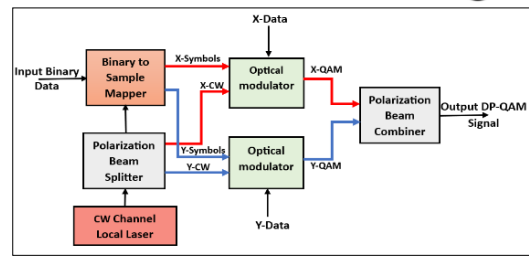
Figure (8): DP-QAM single-channel transmitter (a) and receiver (b).

Table (2): Band's parameters used in the calculations.

Band	T	O	E	S	C	L	U
Used spectrum (THz)	(245-238)	(237-221)	(220-206)	(205-197)	(196-192)	(191-185)	(184-179)
Used BW (THz)	7	16	14	08	04	06	05
N_{ch}	140	320	280	160	80	120	100
α (dB/km)	0.40	0.29	0.24	0.19	0.17	0.18	0.24
D (ps/nm/km)	-06.63	00.0	07.60	13.70	17.00	19.70	22.04
S ps/ (nm^2-km)	0.12	0.07	0.07	0.06	0.06	0.05	0.05
γ (1/W/Km)	1.65	1.58	1.46	1.38	1.30	1.28	1.23

4. Systems Under Consideration

Using UWB-WDM technique with high-order modulation formats over the same existing infrastructure fibers is a promising technique to maximize the data transmission capacity [26]. Therefore, the investigation of fiber characteristic transmission performance is necessary to estimate the transmission capacity boundary and MTR [27]. The traditional numerical simulation of optical fiber communication system uses split-step Fourier method which divides the fiber link into multiple small segments and treats independently the linearity and nonlinearity of each fiber segment [28]. However, this method is inefficient to implement for wide bandwidths systems and/or long-haul links due to the computational effort [29]. Also, the use the fast Fourier transform (FFT) and its inverse fast Fourier transform (IFFT) for every nonlinear step increases the computational complexity for predication the performance of SMF transmission by around 50% [30]. To enable real-time prediction of fiber channel performance in UWB-WDM systems, a closed form approximation of the Gaussian noise model which has been used to predict the performance of these systems, is needed. This method is widely used nowadays since it offers a fast, yet accurate, evaluation of wide-band

range and long-haul distance systems [31], [32] and [33]. According to the enhanced Gaussian noise (EGN) model, the total nonlinear coefficient η_{tot} in $(1/W^2)$ is given by [34]

$$\eta_{tot} \approx \sum_{j=1}^{N_s} \left[\frac{P_{i,j}}{P_i}\right]^2 [\eta_{SPM,i}(f_i) N_s^{\epsilon} + \eta_{XPM,j}(f_i)] \quad \dots(5)$$

where N_s is the number of spans used to construct the optical transmission link, P_i is the power of channel i lunched into the first span, $P_{i,j}$ is the power of channel i launched into jth span, f_i is the relative frequency of the channel of interest, and ϵ is a multispan coherent accumulation factor. The $\eta_{SPM,i}$, and $\eta_{XPM,j}$ is nonlinear interference noise caused by SPM and XPM components, respectively. (See Appendix B for details).

The EGN model has the advantage of offering quickly aid to evaluate the system performance by considering the optical signal-to-noise ratio (OSNR) measure and ignoring the evolution of the temporal waveform over the fiber [27]. The OSNR of ith WDM channel is obtained by [35]

$$OSNR = \frac{P_r}{P_{ASE}+P_{NLI}} \quad \dots(6)$$

In Equation (6), Pr is the received signal channel power and it is related to the input lunch power P_{ch} by $Pr = P_{ch} - \Delta P(z)$, P_{ASE} is the ASE noise power, and $P_{NLI} = \eta_{tot}P_{ch}^3$ is the nonlinear interference noise power. Here P_{ch} presents the channel lunch power which is assumed to be uniform for all channels.

In decibel (dB) scale, the OSNR has a direct relationship with the electrical signal-to-noise ratio SNR [36]

$$OSNR = SNR + 10log_{10}\left(\frac{S_pB_e}{2B_0}\right) \dots(7)$$

where S_p is the number of the polarizations which is equal to 1 for a single polarization and equal to 2 for a dual polarization, B_e is the electrical signal bandwidth, and B_0 is the optical bandwidth. The ratio B_e/B_0 equals 0.5 (double-side optical band), and therefore, the electrical SNR can be computed by

$$SNR = OSNR + 3dB \quad \dots(8)$$

The symbol error rate (SER) corresponding to M-QAM format is given by [37]

$$SER_{M-QAM} = 2\left(1 - \frac{1}{\sqrt{M}}\right) erfc\left(\sqrt{\frac{3\,SNR}{2\,(M-1)}}\right) - \left(1 - \frac{2}{\sqrt{M}} - \frac{1}{M}\right) erfc^2\left(\sqrt{\frac{3\,SNR}{2\,(M-1)}}\right) \quad \dots(9a)$$

where erfc is the standard of the complementary error function. The bit-error rate (BER) performance is measured as a function of the SER [36]

$$BER_{M-QAM} = \frac{1}{log_2(M)}SER_{M-QAM} \quad \dots(9b)$$

For 16-QAM signaling, SER and BER can be deduced from equations 9a and 9b, respectively, as

$$SER_{16-QAM} = \frac{3}{2}erfc\left(\sqrt{\frac{SNR}{10}}\right) - \frac{7}{16}erfc^2\left(\sqrt{\frac{SNR}{10}}\right) \quad \dots(10a)$$

$$BER_{16-QAM} = \frac{1}{4}BER_{16-QAM} \quad \dots(10b)$$

since each 16-QAM symbol has 4 bits ($= log_2(16)$).

Seven DP-16QAM systems are simulated in this work to address the effect of inserting extra bands on the transmission performance and system capacity. The frequency bandwidth and total number of channels carried by each system are listed in Table (3). Note that 1 THz-band grade is inserted between successive bands. It is worth mentioning here that the EGN model evaluates the total NLI η_{tot}, and its SPM and XPM components, $\eta_{SPM,i}$, and $\eta_{XPM,j}$ using the relative frequency "f" concept which indicates the frequency shift from the center frequency of the system band "F_c".

It's worth to mention here that the EGN model described in Equation (5) gives the individual contributions of the nonlinear effects in WDM system to get a closed-form expressions according to [39] and has been used successfully by other research groups [14], [39], [41] and [42]. However, these references consider only two or three-band WDM systems. In our wotk, the EGN model is modified to cover more than three-band system and the main differences are listed in Table (A) (in Appendix A).

Table (3): Bandwidths and total number of channels for the seven UWB-WDM systems under investigation assuming $R_s = 40$ GBaud and $\Delta f = 50$ GHz.

System	System bandwidth (THz)	Total number of WDM channels N_{ch}
C+L	10	200
S+C+L	18	360
S+C+L+U	23	460
E+S+C+L	32	640
E+S+C+L+U	37	740
O+E+S+C+L+U	53	1060
T+O+E+S+C+L+U	60	1200

5. Results and discussion

This section presents simulation results characterize the transmission performance of the seven UWB-WDM systems. The results are given for DP-16QAM signaling, $R_s = 40$ GBaud, and $\Delta f = 50$ GHz. First, the spectral characteristics of total NLI and its SPM and XPM components are reported which is useful to estimate the NLI levels for each channel in the WDM system. Then the dependence of BER on channel lunch power P_{ch} and number of link spans are recorded. These results are used to deduce both the

optimal value of P_{ch} when N_s is fixed and MTR when P_{ch} is fixed. The correct operation of the system should indicate that the BER of each WDM channels is less than a threshold level BER_{th}. A BER_{th} of 3.8×10^{-3} is chosen here which corresponds to a 7% hard decision (HD-forward error correcting (FEC) code [38].

A. Nonlinear interference spectrum

The EGN model is used to obtain the spectra of total nonlinear interference and its SPM and XPM contributions for different UWB-WDM systems and assuming -5 dBm channel lunch power and 1×100 km-span link. The results are presented in Figures (9.a-e) for C2L, S2L, S2U, E2L, and E2U, respectively. The total NLI spectrum shows an increase at the lowest-edge frequency and a decrease at the highest-edge frequency due to SRS effect.

Table (4) summarizes the results depicted from Figures (9.a-e) where the total NLI and its SPM and XPM components are listed at three frequencies for each system. These frequencies denote the lowest-edge frequency f_{LE}, center-bandwidth frequency f_C, and highest-edge frequency f_{HE}.

(a)

(b)

(c)

(d)

(e)
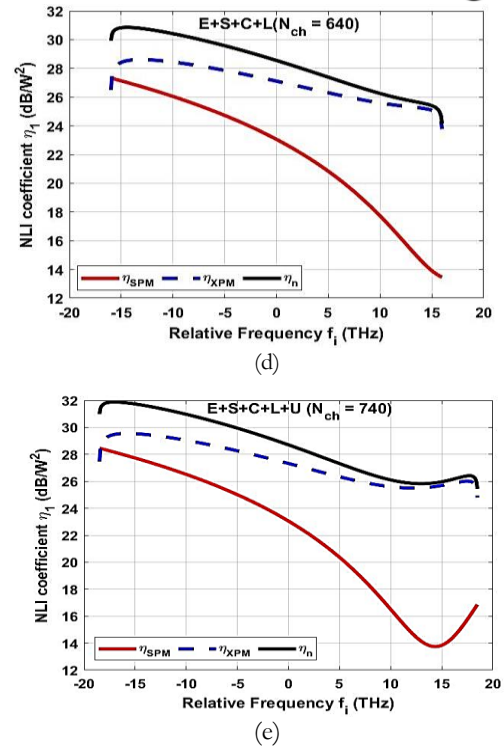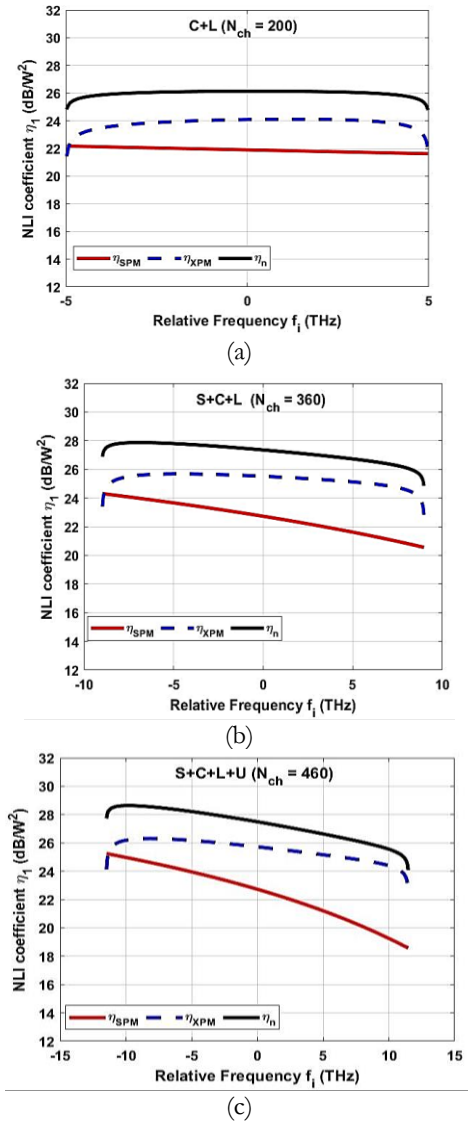
Figure (9): Nonlinear interference of the first five UWB-WDM systems operating with -5 dBm channel power, Dp-16QAM signaling, and 1×100 km-span link (a) C+L, (b) S+C+L, (c) S+C+L+U, (d) E+S+C+L, and (e) E+S+C+L+U.

Table (4): Total nonlinear interference and its SPM and XPM components evaluated for different UWB-WDM systems. $N_s = 1$, $L_s = 100$ km, DP-16QAM, and $\Delta f = 50$ GHz.

(a) Lowest-edge frequency

WDM system	Frequency (THz)		Nonlinear interference NLI (dB/W^2)			
	Relative f_{LE}	Real F_{LE}	η_{SPM}	η_{XPM}	η_N	$\eta_{XPM} - \eta_{SPM}$
C2L	-05.0	186	22.2	21.4	24.8	- 0.8
S2L	-09.0	186	24.3	23.4	26.9	-0.9
S2U	-11.5	180	25.3	24.1	27.7	-1.0
E2L	-16.0	186	27.3	26.5	29.9	-0.8
E2U	-18.5	180	28.4	27.4	30.9	-1.0

(b) Centre band frequency

WDM system	Frequency (THz)		Nonlinear interference NLI (dB/W^2)			
	Relative f_c	Real F_c	η_{SPM}	η_{XPM}	η_N	$\eta_{XPM} - \eta_{SPM}$
C2L	0	192.0	21.9	24.1	26.1	2.2
S2L	0	196.0	22.7	25.5	27.4	2.8
S2U	0	193.0	22.7	24.7	27.5	2.0
E2L	0	203.5	23.1	27.1	28.6	4.0
E2U	0	200.5	24.1	27.8	29.4	3.7

(c) Highest-edge frequency

WDM system	Frequency (THz)		Nonlinear interference NLI (dB/W^2)			
	Relative f_{HE}	Real F_{HE}	η_{SPM}	η_{XPM}	η_N	$\eta_{XPM} - \eta_{SPM}$
C2L	05.0	197	21.6	21.9	24.8	2.2
S2L	09.0	206	20.6	22.8	24.7	2.2

S2U	11.5	206	18.6	22.6	24.1	4.0
E2L	16.0	221	13.5	23.8	24.0	10.3
E2U	18.5	221	13.9	25.5	25.8	11.6

Investigating the results in Table (4) reveals that the total NLI is an increasing function of system bandwidth for the center and lower-edge frequencies. This is because of the increasing in the number of WDM channels which causes an increase in the NLI value due to the increase of the total lunch power. While, the total NLI of the highest-edge frequency decreases with increasing number of channels for C2L, S2L, S2U, and E2L due to the higher power transfer by SRS effect. These results give an idea about how the NLI of a given channel is affected when different extra bands are inserted in the implementation of the UWB-WDM system.

It is worth to estimate the total NLI at specific frequencies for the different systems. The results are listed in Tables (5. a-d) for frequencies F_i =186, 192, 197 and 206 THz, respectively. These values correspond to frequencies in L, L, C, and S bands, respectively. Tables (5. a-c) show an increase in the NLI with the increase of the system bandwidth. Further, Table (5. d) shows that the NLI values depend on the frequencies position in the bands and is related to the amount of power transfer from the channel. In S+C+L and S+C+L+U systems, it lay at the highest-positive edge which its NLI value decreases due to the increase of power transfer from it. Note that the E+S+C+L system has higher NLI value than the above two bands.

The NLI investigation is extended to the other two systems, namely O2U and T2U which use 6 and 7 bands, respectively. The calculations are performed using a fiber span of 50 km length and -8 dBm channel lunch power. The simulation results of the O2U system (1060 channels) and T2U system (1200 channels) are shown in Figures (10 a& b), respectively. The results indicate that the total NLI of the O2U system is 25.5 dB/W^2 and 31 dB/W^2 at the highest- and lowest- frequency edges, respectively. These are to be compared with 25.3 dB/W^2 and 26.3 dB/W^2 for T2U system, respectively.

Table (5): Total nonlinear interference calculated at specific frequencies for different UWB-WDM systems. (System parameters are identical to those given in the caption of Table 4).

(a) F_i = 185 THz

WDM system	f_i (THz)	η_N (dB/W^2)
C2L	-5	24.8
S2L	-9	26.9
S2U	-6	28.3
E2L	-16	29.9
E2U	-13.5	31.5

(b) F_i = 191 THz

WDM system	f_i (THz)	η_N (dB/W^2)
C2L	0	26.1
S2L	-4	27.7

S2U	-1	27.6
E2L	-11.5	30.6
E2U	-8.5	30.7

(c) F_i = 196 THz

WDM system	f_i (THz)	η_N (dB/W^2)
C2L	5.0	24.8
S2L	1.0	27.2
S2U	4.0	27.2
E2L	-6.5	29.8
E2U	-3.5	29.8

(d) F_i = 205 THz

WDM system	f_i (THz)	η_N (dB/W^2)
C2L	Out of range	
S2L	9.0	24.7
S2U	11.5	24.1
E2L	1.5	28.2
E2U	4.5	27.3

(a)

(b)
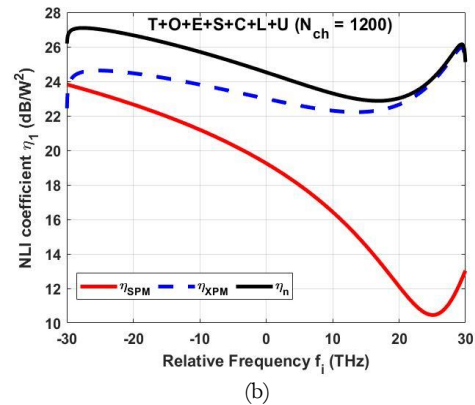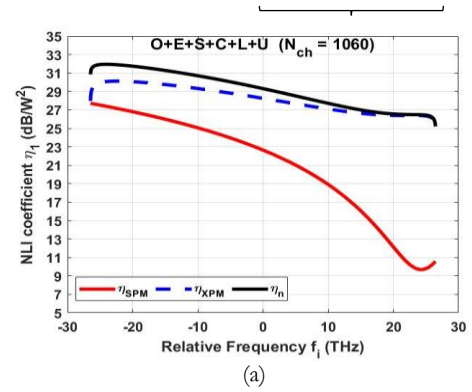
Figure (10): Nonlinear interference of O+E+S+C+L+U system (a) T+O+E+S+C+L+U system (b) assuming DP-16QAM signaling, -8 dBm channel power, and 1×50 km-span link.

B. Power Dependency

The EGN model shows that the nonlinear interaction between the WDM channels has power dependent characteristics since both SPM and XPM components depend on channel launch power as illustrated by Equations (B.1) and (B.2) of Appendix B. It is obvious that the right side of each of these two equations can be separated into two parts, power-dependent and power-independent parts. For the SPM component η_{SPM}

$$\eta_{SPM}(f_i, P_{tot}) = \underbrace{\eta_{SPM-P}(f_i, P_{tot})}_{\text{Power-dependent}} + \underbrace{\eta_{SPM-0}(f_i)}_{\text{Power-independent}}$$

$$.....(11. a)$$

$$\eta_{SPM-0} = (R_i A^2 - E_i \alpha^2) \qquad .....(11. b)$$

$$\eta_{SPM-P}(f_i, P_{tot}) = (E_i - R_i)T_i \qquad ....(11. c)$$

where

$$T_i = (\alpha + \bar{\alpha} - P_{tot} C_r f_i)^2$$

$$A = \alpha + \bar{\alpha}$$

$$E_i = \left(\frac{4}{9} \frac{\gamma^2}{B_i^2} \frac{\pi}{\phi_i \bar{\alpha} \alpha(2\alpha + \bar{\alpha})} \right) \text{asinh}\left(\frac{\phi_i B_i^2}{\pi\alpha} \right)$$

$$R_i = A\left(\frac{4}{9} \frac{\gamma^2}{B_i^2} \frac{\pi}{\phi_i \bar{\alpha} (2\alpha+\bar{\alpha})} \right) \text{asinh}\left(\frac{\phi_i B_i^2}{\pi A} \right)$$

For the XPM component η_{XPM}

$$\eta_{XPM}(f_i, P_{tot}) = \underbrace{\eta_{XPM-P}(f_i, P_{tot})}_{\text{Power-dependent}} + \underbrace{\eta_{XPM-0}(f_i)}_{\text{Power-independent}}$$

$$.....(12. a)$$

$$\eta_{XPM-0}(f_i) = \frac{32}{27} \sum_{k=1 \ k \neq i}^{N_{ch}} (\Gamma_k A^2 - \Psi_k \alpha^2) \quad ...(12. b)$$

$$\eta_{XPM-P}(f_i, P_{tot}) = \frac{32}{27} \sum_{k=1 \ k \neq i}^{N_{ch}} \{(\Psi_k - \Gamma_k + S)T_k\}$$

$$....(12.c)$$

where

$$T_k = (\alpha + \bar{\alpha} - P_{tot} C_r f_k)^2$$

$$\Psi_k = \frac{\gamma^2}{B_k} \frac{\text{atan}\left(\frac{\phi_{i,k} B_i}{A} \right)}{A} \frac{N_s + \frac{5}{6}\Phi}{\phi_{i,k} \bar{\alpha} (2\alpha + \bar{\alpha})}$$

$$F_k = \frac{\text{atan}\left(\frac{\phi_{i,k} B_i}{A} \right)}{A}$$

$$S = \frac{\gamma^2}{B_k} \frac{5}{3} \frac{\Phi \pi \tilde{N}}{|\phi| B_k^2 \alpha^2 A^2} [2|\Delta f| - B_k) \log(\frac{2|\Delta f| - B_k}{2|\Delta f| + B_k}) + 2B_k]$$

Therefore, the η_{SPM} at the center of the system bandwidth ($f_i = 0$) is equal to $\eta_{SPM}(0) = \eta_{SPM-0}(0)$, and its value does not depend on the channel lunch power. The $\eta_{XPM}(0)$ has negligible dependence on channel lunch power.

Figure (11) shows the NLI spectrum of S+C+L UWB-WDM system computed at three different lunch powers, -6, -4, and -2 dBm. It can be noticed that the NLI at $f_i = 0$ is almost constant with difference of 0.02 dB/W^2 between -6 and -4 dBm lunch powers and 0.04 dB/W^2 between -4 and -2 dBm lunch powers. Therefore, at $f_i = 0$ (center of the system bandwidth) the optimal power can be obtained depending on Equation (6) and by ignoring the power dependency at this frequency. Then by differentiating the OSNR with respect to P_{ch} and setting the result to zero, one can obtain the optimal channel power $(P_{ch})_{opt}$

$$\frac{dOSNR}{dP_{ch}} = \frac{(P_{ASE} + \eta P_{ch}^3) - P_i(3(d\eta/dp)P_{ch}^2)}{(P_{ASE} + \eta P_{ch}^3)^2} \qquad .....(13)$$

Then the optimal power at $f_i = 0$ is equal to

$$(P_{ch})_{opt} = \sqrt[3]{\frac{P_{ASE}}{2\eta}} \qquad .....(14)$$

However, the most channel affected by NLI is the highest-edge frequency channel. It is expected that this channel has the highest BER among the whole channels due to the influence of SRS. The variation of the BER of the highest-frequency channel is investigated for the seven UWB-WBM systems and the results are depicted in Figure (12). Parts a-e of this figure correspond to C2L, S2L, S2U, E2L, and E2U systems, respectively, and assuming a 100 km-span length. Parts a and b of Figure (13) correspond to O2U and T2U systems, respectively, and assuming $L_s = 50$ km. The number of spans N_s used to construct the transmission link is taken as an independent parameter in these figures. The OAS used in the WDM systems of Figure (12) has up to five optical amplifiers (according to the number of used bands) with gains $G_E = 24$, $G_S = 19$, $G_C = 17$, $G_L = 18$, and $G_U = 24$ dB. (Here the subscript denotes the band). In Figure (13), the OAS uses six or seven optical amplifiers; the extra OAs have gains $G_O = 14.5$ dB and $G_T = 20$ for the sixth and seven band, respectively.
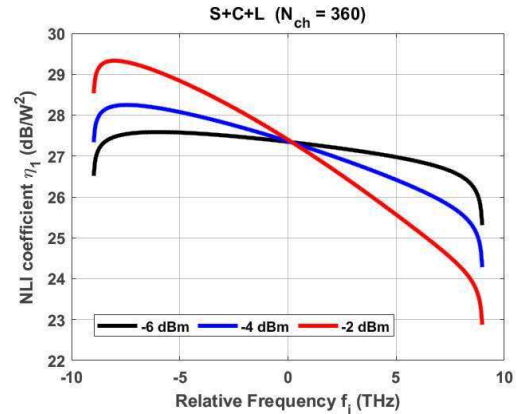
Figure (11): Nonlinear interference of DP-16QAM S+C+L system for different channel lunch power and assuming 40 GBaud symbol rate, 50 GHz channel spacing, and 1×100 km-span link.

The results in Figures (12 and 13) are presented for the highest-frequency channel, which is expected to have the highest BER among the channels, and for $Ns = 1, 2,$ and 3 spans. Investigating the results in these figures reveals that there is an optimal lunch power $(P_{ch})_{opt}$ which minimizes the BER. The deduced values of $(P_{ch})_{opt}$ are -4, -5, -5, -4.5 and -3.5 dBm for C2L, S2L, S2U, E2L, E2U systems, respectively, and $(P_{ch})_{opt} = -6$ and -4.5 for O2U and T2U systems, respectively. The results also indicate that the optimal channel power is almost not affected by the number of spans, and it reduces by about -1 dBm for C2L and E2U systems when a 20×100 km-span link and 4×100 km-span link is used, respectively. Note further that the BER increases with increasing number of spans for

all the seven systems. Recall that the BER characteristics of the highest-frequency channel is kept under observation to estimate $(P_{ch})_{opt}$. Therefore, one needs to check that all the WDM channels operate with $BER < BER_{th}$ when all have identical lunch power, $P_{ch} = (P_{ch})_{opt}$. This is illustrated in Figures (14.a-h) where the BER is reported for each WDM channel of the seven systems. Using $(P_{ch})_{opt}$ of -5 dBm for C2L, S2L, and S2U systems give a maximum reach of 19, 9, and $9 \times 100\ km-span$, respectively. Using -4.5 dBm channel lunch power for E2L and E2U systems gives a maximum reach of 4×100 km-span. Using -7 dBm for O2U and -5 dBm for T2U systems gives a maximum reach of 22×50 km-span and 3×50 km-span, respectively.

(a)

(b)

(c)

(d)

(e)
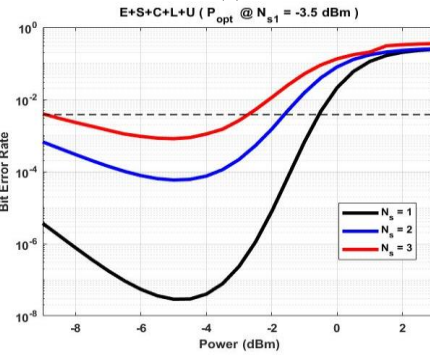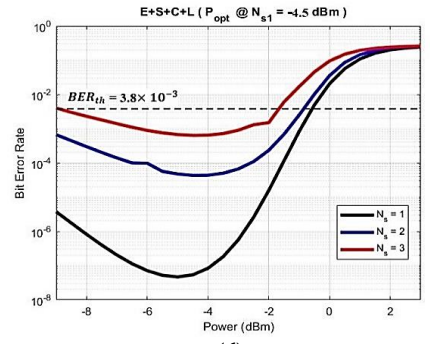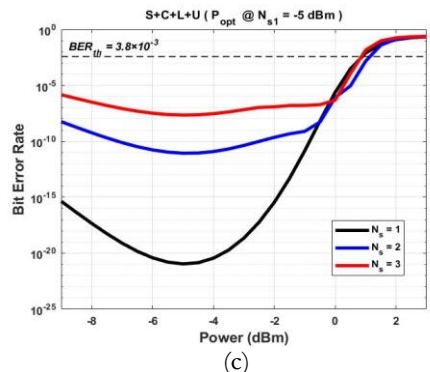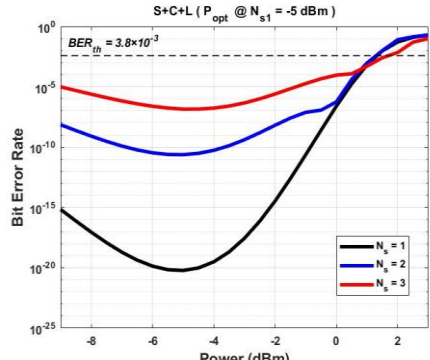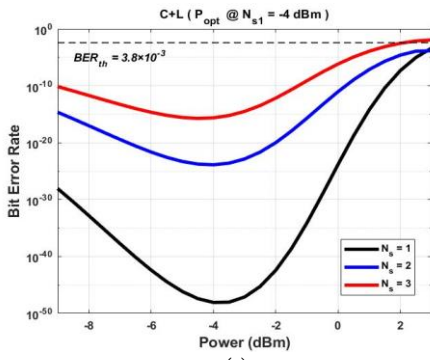
Figure (12): Variation of BER with channel lunch power for DP-16QAM UWB-WDM system operating with Rs = 40 GBaud, Δf = 50 GHz, and Ls = 100 km (a) C2L, (b) S2L, (c) S2U, (d) E2L, and (e) E2U.

(a)

(b)
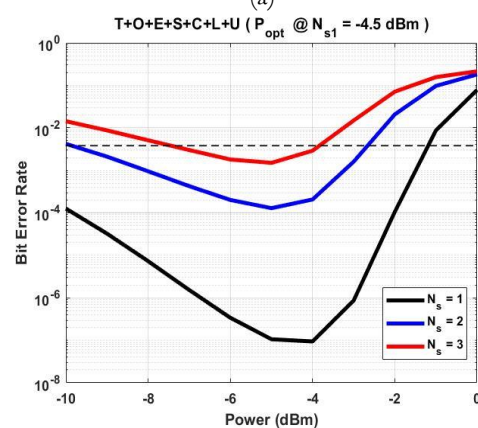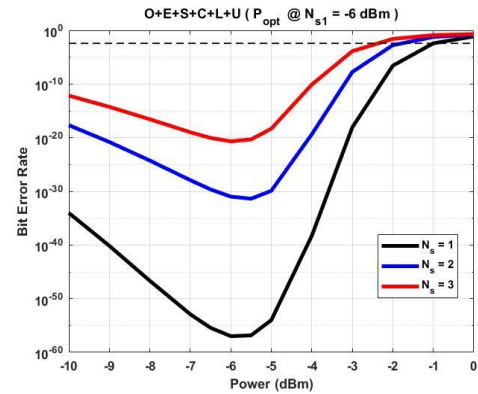
Figure (13): Variation of BER with channel lunch power for O2L (a) and T2U (b) systems operating with Rs = 40 GBaud, Δf = 50 GHz, and Ls = 50 km.

(a)

(b)

(c)

(d)

(e)

(f)

(g)
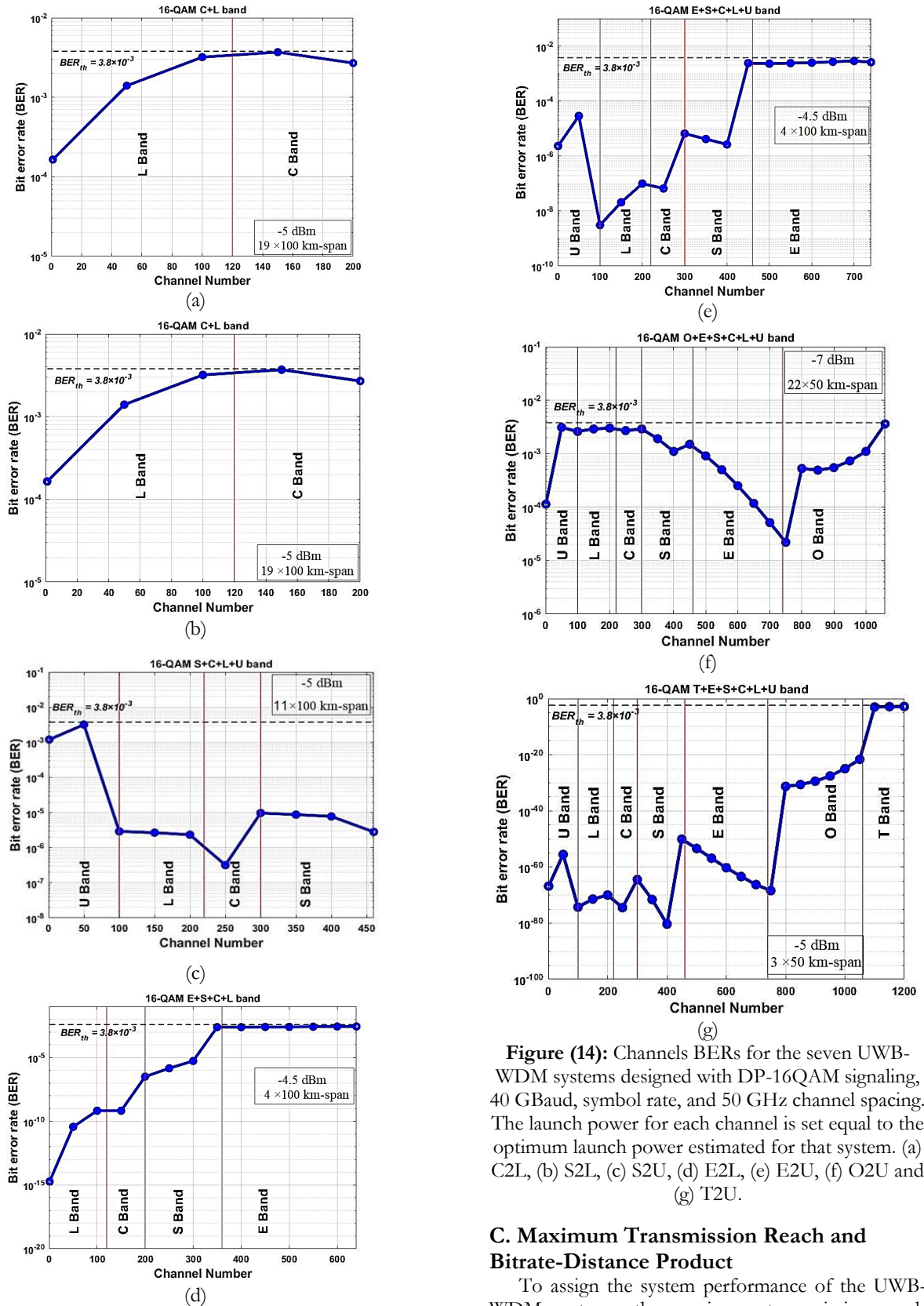
Figure (14): Channels BERs for the seven UWB-WDM systems designed with DP-16QAM signaling, 40 GBaud, symbol rate, and 50 GHz channel spacing. The launch power for each channel is set equal to the optimum launch power estimated for that system. (a) C2L, (b) S2L, (c) S2U, (d) E2L, (e) E2U, (f) O2U and (g) T2U.

C. Maximum Transmission Reach and Bitrate-Distance Product

To assign the system performance of the UWB-WDM systems, the maximum transmission reach (MTR) is used as one of the measures. MTR indicates the maximum number of spans (or maximum fiber length) that can be used to construct the transmission link while keeping BER less than a specified threshold value BER_{th}. It is worth to mention here that MTR depends on channel lunch power P_{ch}. Three different values of P_{ch} (-2, -5 and -7 dBm) are considered for first five systems assuming R_s= 40 Gabud, Δf=50

GHz and L_s = 100 km. Figures (15.a and b) show the MTR and bit rate -distance product (BDP), respectively, for C2L, S2L, S2U, E2L and E2U systems. The simulation is repeated for O2U and T2U systems using 50 km-span length and the results are depicted in Figures (16 a and b). Three values of P_{ch} (-2, -5 and -7 dBm) are considered here. The results show that the highest values of MTR and BDP are obtained in the O2U system when P_{ch} = -5 dBm. (MTRmax = 33× 50 km-span and BDPmax = 11193 Tbps.km).
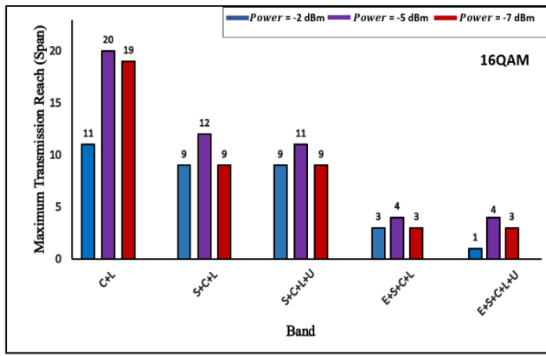
(a)
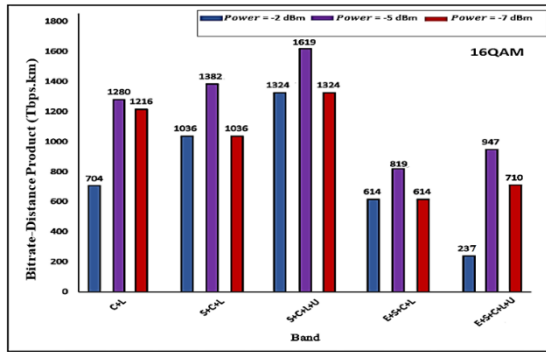
(b)

Figure (15): Number of maximum reach spans (a) and bit rate-distance product (b) of C+L, S+C+L, S+C+L+U, E+S+C+L, and E+S+C+L+U systems and assuming DP-16QAM signaling, Ls = 100 km, R_s = 40 GBaud and Δf = 50 GHz.

6. Challenges Facing the Implementation of UWB-WDM Systems

The implementation of UWB-WDM systems, which operate over a large frequency range and carry high transmission data rate, will rely on the existing infrastructure fibers to reduce the cost. Although, UWB-WDM communication systems offer many advantages, but also face several challenges. Addressing these challenges requires innovative solutions and careful system design to ensure reliable and robust communication

I. Crosstalk between channels: In a UWB-WDM communication system, large number of channels with closely frequency spacing is used. This can result in crosstalk between the neighboring channels. Crosstalk can cause interference and reduce the overall system performance.

II. Complexity of system design: UWB communication systems require careful design of complex components systems such as advanced signal processing, UWB optical transmitters, and UWB optical receivers. The wide bandwidth of UWB signals also requires high sampling rates, which can increase the computational complexity of the system. Also, the main components for optical UWB transceivers are not available as commercial products such as [80]; UWB tunable laser, UWB dual-polarization IQ modulator, and UWB coherent receiver front end.

III. Power consumption: The power consumption of the individual components in the UWB-WDM communication system, such as lasers, modulators, and amplifiers, can significantly impact the overall power consumption. Therefore, it is essential to optimize the power consumption of each component to achieve the desired power efficiency.

IV. Signal-to-noise ratio (SNR) requirements: UWB-WDM communication systems typically require high SNR levels to ensure reliable communication. Achieving high SNR levels often requires the use of high-power components, which can increase the overall power consumption and his cause to increase the nonlinear channel interface.

V. Optical amplifiers: Design optical amplifier scheme with lowest number of optical amplifiers is great challenges for UWB-WDM system.
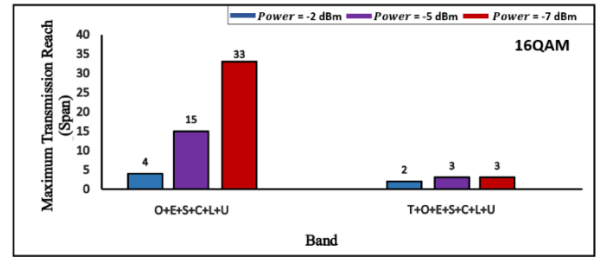
(a)
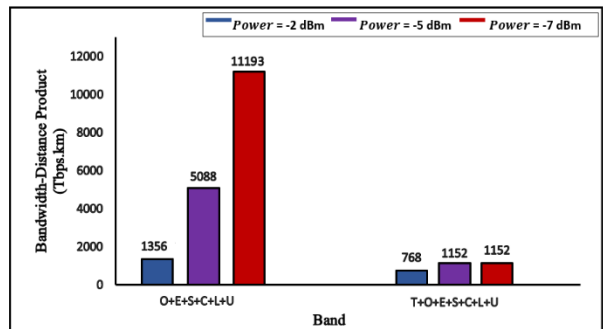
(b)

Figure (16): (a) Number of maximum reach spans, (b) Bandwidth-distance product of DP-16QAM of (a) O+ E+S+C+L+U and (b) T+O+ E+S+C+L+U for Ls = 50 km, Rs = 40 GBaud and Δf = 50 GHz.

4. Conclusions

This paper has discussed the design considerations and performance estimation of various coherent UWB-WDM systems. Seven systems have been investigated using a 40 GBaud symbol rate, 50 GHz channel frequency spacing, and DP-16QAM signaling. To optimize system performance and minimize BER, trade-off between different system parameters, (such as the number of channels, channel spacing,

transmission distance, optical OSNR, modulation format, and nonlinear fiber effects) should be considered. considered.

The variation of the BER of the highest-frequency channel with channel lunch power P_{ch} investigated for the seven UWB-WBM systems. The first five systems C2L, S2L, S2U, E2L, and E2U can be implemented with 100 km fiber length because they having lower accumulated nonlinearity, lower number of channels, than O2U and T2U systems. However, O2U and T2U can be propagated with fiber link of 50 km due its high NLI obtained from the high number of channels.

Further, the highest MTR can be obtained with C2L WDM system operating over 20×100 km-spans due to its lower NLI value making it further propagate for higher distance. However, the maximum BDP can be obtained with S2U WDM system.

Acknowledgments

Appendix A
Summary of the UWB-WDM Communication Systems reported in the Literate

Table (A): Summary of UWB-WDM transmission systems investigated in the literature.

Band	Year and Ref.	Modulation format	Remarks			Transmission distance	Investigated points			Type of study
			Symbol rate (Gbaud)	Channel spacing (GHz)	Number of WDM channels		Opt. power	BER	Frequency dependent parameters	
C	2023 [4]	DP-16QAM	16 32 64 128	16 32 64 128	281 141 71 35	5800 km 5700 km 5100 km 4660 km	done	-	done	Theo.
	2023 [41]	PM-QPSK PM-64QAM	32	50	80	500 km	-	-	done	Theo.
	2022 [42]	DP-QPSK, DP-16QAM, DP-64QAM, and DP- 256QAM	32 48 64 128	32 48 64 128	61 51 33 15	11000 km	done	-	done	Theo.
	2022 [43]	DP-16QAM	64	75	54	60 km	-	-	done	Theo.
C2L	2022 [5]	DP-16QAM	120	125	15, 25 and 45	3000 km	done	-	-	Theo.
	2022 [6]	PM-16QAM PM-32QAM PM-64QAM	24.5	25	424	234.8 km	done	-	done	Theo. & Exp.
	2022 [43]	DP-16QAM	64	75	146	60 km	-	-	done	Theo.
	2023 [44]	DP-16QAM	64	100	96	980 km - Theo. 680 km - Exp.	-	-	done	Theo. & Exp.
	2020 [14]	PM-QPSK and PM-16QAM PM-QPSK and PM-16QAM	32 43	50 75	220 147	960 km	-	-	done	Theo.
	2022 [45]	PM-QPSK DP-16QAM	64	75	146	60 km	-	-	-	Theo.
	In this work	DP-16QAM	40	50	200	2000 km	done	done	done	Theo.
S+L	2020 [46]	16QAM	32	100 in S 50 in L	75	210 km	-	-	done	Exp.
S2L	2022 [43]	DP-16QAM	64	75	271	60 km	-	-	done	Theo.
	2020 [14]	PM-QPSK and PM-16QAM PM-QPSK and PM-16QAM	32 43	50 75	402 268	960 km	-	-	done	Theo.

Band	Year and Ref.	Modulation format	Remarks			Transmission distance	Investigated points			Type of study
			Symbol rate (Gbaud)	Channel spacing (GHz)	Number of WDM channels		Opt. power	BER	Frequency dependent parameters	
	2023 [32]	Gaussian Modulation	64	75	277	1000 km	-	-	done	Theo.
	2022 [9]	DP-256QAM	24.5	25	793	54 km	-	-	done	Exp.
	2022 [47]	QAM	32	50	400	7500 km	-	-	-	Theo.
	2022 [48]	16QAM and 64QAM	49	50	247	257.5 km	-	-	done	Exp.
	2022 [45]	PM-QPSK DP-16QAM	64	75	271	60 km	-	-	-	Theo.
	2022 [7]	DP-16QAM	40	50	360	1200 km	done	done	done	Theo.
S2U	2022 [13]	16QAM	64	75	256 320	75 km	-	-	-	Theo.
	In this work	DP-16QAM	40	50	460	1100 km	done	done	done	Theo.
E+C+L	2022 [45]	PM-QPSK DP-16QAM	64	75	292	60 km	-	-	-	Theo.
	2022 [43]	DP-16QAM	64	75	292	60 km	-	-	done	Theo.
E2L	2023 [32]	Gaussian Modulation	64	75	479	1000 km	-	-	done	Theo.
	2022 [49]	PM-16QAM	30	100	150	70 km	-	-	done	Exp.
	2020 [14]	PM-QPSK and PM-16QAM PM-QPSK and PM-16QAM	32 43	50 75	698 465	960 km	-	-	done	Theo.
	In this work	DP-16QAM	40	50	640	400 km	done	done	done	Theo.
E2U	In this work	DP-16QAM	40	50	740	400 km	done	done	done	Theo.
O2L	2020 [14]	PM-QPSK and PM-16QAM PM-QPSK and PM-16QAM	32 43	50 75	938 625	960 km	-	-	done	Theo.
	2020 [20]	The modulation format is adaptable. i.e., a bit-loading technique is supposed	32	50	937	600 km	done	-	done	Theo.
O2U	2022 [50]	Suggested as silicon TE-pass polarizer based on ridge waveguide adiabatic S-bends								
	In this work	DP-16QAM	40	50	1060	1650 km	done	done	done	Theo.
T2U	In this work	DP-16QAM	40	50	1200	150 km	done	done	done	Theo.

Appendix B
Summary of the Enhanced Gaussian Noise (EGN) Model

The EGN model has been applied in the literature for multispan C+L and S+C+L WDM systems and has been adopted in this paper for the other five systems. The nonlinear interference (NLI) noise can be considered as an additive Gaussian noise and resolved by the EGN assumption model. NLI noise is governed by two contributions, SPM and XPM, as shown in Equation (5). The SPM and XPM contributions are given by [29]

$$\eta_{SPM}(f_i) \approx \frac{4}{9} \frac{\gamma^2}{B_i^2} \frac{\pi}{\phi_i \, \bar{\alpha} \, (2\alpha + \bar{\alpha})} \cdot \left[\frac{T_i - \alpha^2}{\alpha} \text{asinh}\left(\frac{\phi_i \, B_i^2}{\pi \alpha}\right) + \frac{A^2 - T_i}{A} \text{asinh}\left(\frac{\phi_i \, B_i^2}{\pi A}\right) \right] \quad \text{(B. 1)}$$

where $\phi_i = \frac{3}{2}\pi^2\left(\left(-\frac{\lambda^2 D}{2\pi c}\right) + \left(\frac{2\lambda^3 D f_i}{2\pi c^2}\right)\right)$, $A = \alpha + \bar{\alpha}$ and $T_i = (\alpha + \bar{\alpha} - P_{tot}C_r f_i)^2$

$$\eta_{XPM}(f_i) \approx$$
$$\frac{32}{27}\sum_{k=1 \; k\neq i}^{N_{ch}}\left(\frac{P_k}{P_i}\right)^2\frac{\gamma^2}{B_k}\left\{\frac{N_s + \frac{5}{6}\Phi}{\phi_{i,k}\bar{\alpha}(2\alpha + \bar{\alpha})}\cdot\left[\frac{T_k - \alpha^2}{\alpha}\text{atan}(\frac{\phi_{i,k}B_i}{\alpha}) + \frac{A^2 - T_k}{A}\text{atan}(\frac{\phi_{i,k}B_i}{A})\right] + \frac{5}{3}\frac{\Phi\pi\breve{N}T_k}{|\phi|B_k^2\alpha^2 A^2}\left[(2|\Delta f| - B_k)\log(\frac{2|\Delta f| - B_k}{2|\Delta f| + B_k}) + 2B_k\right]\right\} \quad\quad\dots\dots(B.2)$$

The parameter $\breve{N}$ in Equation (A.2) depends on the number of spans N_s

$$\breve{N} = \begin{cases} 0, & if \; N_s = 1 \\ N_s, & otherwise \end{cases} \quad\dots\,(B.3)$$

The Kurtosis parameter (i.e., the modulation factor Φ) is defined as in [40] $\Phi = (E\{|x|^4\}/E^2\{|x|^2\}) - 2$, where x denotes the data symbol and E is the expectation operator. The modulation factor Φ is equal to -0.68 for 16-QAM [8]. Further, $T_k = (\alpha + \bar{\alpha} - P_{tot}C_r f_k)^2$ and $\phi_{i,k} = -2\pi^2(f_k - f_i)((-\lambda^2 D/(2\pi c) + (2\lambda^3 D f_i/(2\pi c^2)))$. where, f_i

and f_k are the relative frequencies of the interested ith channel and the interfering kth channel, respectively. To simplify the calculations, the attenuation parameter α is assumed equals to the average attenuation $\bar{\alpha}$ [28]. Note that ϕ_i and $\phi_{i,k}$ correspond to SPM at frequency f_i and XPM between the two frequencies i and k, respectively. Furthermore, B_i & B_k is the bandwidth of i and k channel, respectively, Δf frequency spacing, P_{tot} is the total channels lunch power.

6. References

[1] W. Shi, Y. Tian, and A. Gervais, "Scaling Capacity of Fiber-Optic Transmission Systems Via Silicon Photonics", Nanophotonics, vol. 9, no. 16, pp. 4629–4633, 2020, doi: 10.1515/nanoph-2020-0309.

[2] V. Lopez, B. Zhu, D. Moniz, N. Costa, J. Pedro, X. Xu, A. Kumpera, L. Dardis, J. Rahn, and S. Sanders, "Optimized Design and Challenges for C&L Band Optical Line Systems", Journal of Lightwave Technology, vol. 38, no. 5, pp. 1080–1091, 2020, doi: 10.1109/JLT.2020.2968225.

[3] F. H. Tithi and S. P. Majumder, "Analytical Evaluation of Combined Influence of XPM, ASE and SRS in A Raman Amplifier Based WDM System", Optik., vol. 208, Artical no. 164076, pp. 1–15, 2020, doi: 10.1016/j.ijleo.2019.164076.

[4] T. Jin, Cenqin Shevchenko, Nikita A. Wang, Junqiu Chen, Yunfei Xu, "Wideband Multichannel Nyquist-Spaced Long-Haul Optical Transmission Influenced by Enhanced Equalization Phase Noise", Sensors, vol. 23, no. 3, pp. 1–10, 2023, doi: 10.3390/s23031493.

[5] M. Dahan, David Zarubinsky, Michael Liang, Yunhua Golani, Ori Shtaif, "Universal Virtual Lab: A Fast and Accurate Simulation Tool for Wideband Nonlinear DWDM Systems", Journal of Lightwave Technology, vol. 40, no. 8, pp. 2441–2455, 2022, doi: 10.1109/JLT.2022.3141447.

[6] H. Luis, Ruben S. Puttnam, Benjamin J. Rademacher, G. Awaji, Y. Furukawa, "Demonstration of A 90 Tb/S, 234.8 km, C+L Band Unrepeated SSMF Link with Bidirectional Raman Amplification", Optics Express, vol. 30, no. 8, pp. 13114–13118, 2022, doi: 10.1364/oe.451948.

[7] A. A. Moosa and R. S. Fyath, "Effect of Fiber Stimulated Raman Scattering on the Performance of of S+C+L Ultra-wideband WDM System," 2022 Iraqi International Conference on Communication & Information Technologies (IICCIT-2022) , Basrah University , Basrah , Iraq, 2022, doi: 10.1109/IICCIT55816.2022.10010481.

[8] A. Moosa and R. S. Fyath, "Performance Investigation of DP-16QAM Ultra-wideband-Wavelength-Division Multiplexing Communication System: Optimum Power Consideration", Al-Nahrain Journal for Engineering Sciences, vol. 26, no. 1. pp. 37–44, 2023, doi:https://doi.org/10.29194/NJES.26010037.

[9] B. J. Puttnam, G. Ruben S. Luís, A. H. F. Rademacher, M. Mendez-Astudillio, and Y. Awaji, "S-, C- and L-Band Transmission Over A 157 nm Bandwidth Using Doped Fiber and Distributed Raman Amplification", Optics Express, vol. 30, no. 6, pp. 10011–10017, 2022, doi: https://doi.org/10.1364/OE.448837.

[10] A. A. Moosa and R. S. Fyath, "Detailed Performance Investigation and BER Characterization of S+C+L Band-WDM Transmission System", Optik, vol. 276, Article no. 170641, pp. 1–17, 2022, doi: https://doi.org/10.1016/j.ijleo.2023.170641.

[11] S. Al-Azzawi, Alabbas A. Almukhtar, Aya A. Hmood, Jassim K. Das and S. W. Dhar, A. Paul, M. C. Harun, "Broadband ASE Source for S + C + L Bands Using Hafnia-Bismuth Based Erbium Co-Doped Fibers", Optik, vol. 255, Article no. 168723, pp. 1–6, 2022, doi: 10.1016/j.ijleo.2022.168723.

[12] M. S. Habib, M. M. Haque and S. M. A. S. Habib, M. Hasan, M. I. S. Rahman, and M. Razzak, "Polarization Maintaining Holey Fibers for Residual Dispersion Compensation Over S + C + L Wavelength Bands", Optik, vol. 125, no. 3, pp. 911–915, 2014, doi: 10.1016/j.ijleo.2013.04.133.

[13] B. Sadeghi, Rasoul Correia and V. Virgillito, Emanuele Napoli, Antonio Costa, Nelson Pedro, Joao Curri, "Optimal Spectral Usage and Energy Efficient S-to-U Multiband Optical Networking", in 2022 Optical Fiber Communications Conference and Exhibition, OFC 2022 - Proceedings, 2022, pp. 1–3. doi: 10.1364/ofc.2022.w3f.7.

[14] A. Sambo, N. Ferrari, N. Napoli, A. Costa, and V. Pedro, J. Sommerkorn-Krombholz, B. Castoldi, Piero Curri, "Provisioning in Multi-Band Optical Networks," Journal of Lightwave

Technology, vol. 38, no. 9, pp. 2598–2605, 2020, doi: 10.1109/JLT.2020.2983227.

[15] Z. Wang, X. y. Li, S. G. Liu, and Q. Fan, "Ultra-Broadband Polarization Filter Covering O + E + S + C + L + U Telecom Wavebands Based on Au-Coated Photonic Crystal Fiber", Optik, vol. 156, pp. 463–469, 2018, doi: 10.1016/j.ijleo.2017.11.007.

[16] J. Palais, "Fiber Optic Communications Systems", USA: Springer, 2021. doi: 10.1201/9781420041163-49.

[17] K. Minoguchi , M., Kyo, H. Fukutaro, S. Okamoto, T. Sasai, K.Horikoshi, A. Matsushita, M. Nakamura, Masanori, E. Yamazaki, Etsushi.Y. Kisaka, Yoshiaki, "Beyond 100-Tb/S Ultra-Wideband Transmission in S, C, And L Bands Over Single-Mode Fiber", SPIED,p. 18, 2020, doi: 10.1117/12.2541990.

[18] G. C. Salma Escobar Landero, I. F. de Jauregui Ruiz, A.Ferrari, D. Le Gac, Y. Frignac, "Link Power Optimization for S+C+L Multi-Band WDM Coherent Transmission Systems", 2022 Optical Fiber Communication (OFC) Conference, Optica Publishing, 2022, pp. 1–3. doi: 10.1364/ofc.2022.w4i.5.

[19] G. D'Amico, A. Correia, B. London, E.Virgillito, E. Borraccini and V. Napoli, A. Curri, "Scalable and Disaggregated GGN Approximation Applied to a C+L+S Optical Network", Journal of Lightwave Technology, vol. 40, no. 11, pp. 3499–3511, 2022, doi: 10.1109/JLT.2022.3162134.

[20] A. Ferrari, A. Napoli, J.K. Fischer, N. Costa, A. D'Amico, J. Pedro, W. Forysiak, E. Pincemin, A. Lord, A. Stavdas, J.F.P. Gimenez, G. Roelkens, N. Calabretta, S. Abrate, B. Sommerkorn-Krombholz, V. Curri, "Assessment on the achievable throughput of multi-band ITU-T G.652.D fiber transmission systems", Journal of Lightwave Technology, vol. 38, pp. 4279–4291, 2020 https://doi.org/10.1109/JLT.2020.2989620.

[21] L. N. Binh, "Optical fiber communications systems: Theory and practice with matlab® and simulink® " models. CRC Press, 2015.

[22] F. M. Mustafa, M. M. Abdelhalim, and M. H. Aly, "Dispersion Compensation: Impact of Integration of Soliton Transmission and Cascaded Apodized FBGs", Optical and Quantum Electronics, 2022, doi: 10.1007/s11082-022-04188-4.

[23] M. F. S. Ferreira, "Optical Signal Processing in Highly Nonlinear Fibers", London New York: CRC Press, 2020.

[24] N. N. A. Shevchenko, S. Nallaperuma, and S. J. Savory, "Maximizing the Information Throughput of Ultra-Wideband Fiber-Optic Communication Systems", Optics Express, vol. 30, no. 11, p. 19320, 2022, doi: 10.1364/oe.447591.

[25] G.G.P. AGRAWAL. "Nonlinear Fiber Optics", 6th Edition, Elsevier Accadimic Press, 2019.

[26] R. Emmerich, M. Sena, R. Elschner, C. Schmidt-Langhorst, I. Sackey, C. Schubert, and R. Freund, "Enabling S-C-L-Band Systems with Standard C-Band Modulator and Coherent Receiver Using Coherent System Identification and Nonlinear Predistortion", Journal of Lightwave Technology, vol. 40, no. 5, pp. 1360–1368, 2022, doi: 10.1109/JLT.2021.3123430.

[27] J. L. Gao Ye, J. Xiang, G. Zhou, M. Xiang and A. S. F. Yuwen Qin, "Impact of the Input OSNR on Data-Driven Optical Fiber Channel Modeling", Optical Communications and Networking, vol. 15, no. 2, pp. 78–86, 2023, doi: 10.1364/JOCN.476195.

[28] X. Lin, S. Luo, S.K.O. Soman, L. Lampe, D. Chang, Ch Li, "Perturbation Theory-Aided Learned Digital Back-Propagation Scheme for Optical Fiber Nonlinearity Compensation", Journal of Lightwave Technology, vol. 40 , pp. 1981–1988, 2022 https://doi.org/10.1109/JLT.2021.3133475.

[29] C. Lasagni, P. Serena, and A. Bononi, "Modeling Nonlinear Interference with Sparse Raman-Tilt Equalization," Journal of Lightwave Technology, vol. 39, no. 15, pp. 4980–4989, 2021, doi: 10.1109/JLT.2021.3082287.

[30] D. Semrau, E. Sillekens, R. I. Killey, and P. Bayvel, "Modelling the Delayed Nonlinear Fiber Response in Coherent Optical Communications," Journal of Lightwave Technology, vol. 39, no. 7, pp. 1937–1952, 2021, doi: 10.1109/JLT.2020.3046998.

[31] H. Buglia, M. Jarmolovi˘cius, A. Vasylchenkova, E. Sillekens, L. Galdino, R. I. Killey, and P. Bayvel, "A Closed-Form Expression for the Gaussian Noise Model in the Presence of Inter-Channel Stimulated Raman Scattering Extended for Arbitrary Loss and Fibre Length," Journal of Lightwave Technology, vol. PP, pp. 1–10, 2023, doi: 10.1109/jlt.2023.3256185.

[32] J. C. Lasagni, C. Serena, P., A. Antona, "A Generalized Raman Scattering Model for Real-Time SNR Estimation of Multi-Band Systems," Journal of Lightwave Technology, pp. 1–11, 2023, doi: 10.1109/JLT.2023.3250751.

[33] P. Poggiolini and M. Ranjbar-Zefreh, "Closed Form Expressions of the Nonlinear Interference for UWB Systems," 2022 European Conference on Optical Communication, ECOC 2022, pp. 1–4, 2022.

[34] D. Semrau, E. Sillekens, P. Bayvel, and R. I. Killey, "Modeling and mitigation of fiber nonlinearity in wideband optical signal transmission," Journal of Optical Communications and Networking, vol. 12, no. 6, pp. C68–C76, 2020, doi: 10.1364/JOCN.382267.

[35] A. Souza, N. Costa, J. Pedro, and J. Pires, "Benefits of Counterpropagating Raman Amplification for Multiband Optical Networks," Journal of Optical Communications and Networking, vol. 14, no. 7, p. 562, 2022, doi: 10.1364/jocn.456582.

[36] F. Wu, Tianze Tian, Y. Wu, X. Yue, Y. Gu, Y. Cui, and Q. Zhang, "Performance Analysis and Power Tilt Mitigation of Ultra-Wideband WDM Transmission Systems," Photonics, vol. 10, no.

5, pp. 1–19, 2023, doi: https://doi.org/10.3390/photonics10050530.

[37] P. System, S. Qam, Y. V. Kryukov, and D. A. Pokamestov, "Symbol Error-Rate Analytical Expressions for a Two-User PD-NOMA System with Square QAM", Symmetry, vol. 13, Article no. 2153, pp. 1–13, 2021, doi: https://doi.org/10.3390/sym13112153.

[38] H. K. Chan, D.W.U., Wu, Xiong, Z. Zunyue, Lu, C. Lau, A. Pak, T. Tsang, "Ultra-Wide Free-Spectral-Range Silicon Microring Modulator for High Capacity WDM", Journal of Lightwave Technology, vol. 40, no. 24, pp. 7848–7855, 2022, doi: 10.1109/JLT.2022.3208745.

[39] E. Semrau, Daniel, Sillekens and P. Killey, Robert I., Bayvel, "A Modulation Format Correction Formula for the Gaussian Noise Model in the Presence of Inter-Channel Stimulated Raman Scattering," Journal of Lightwave Technology, vol. 37, no. 19, pp. 5122–5131, 2019, doi: 10.1109/JLT.2019.2929461.

[40] A. Soleimanzade and M. Ardakani, "EGN-Based Optimization of the APSK Constellations for the Non-Linear Fiber Channel Based on the Symbol-Wise Mutual Information," Journal of Lightwave Technology, vol. 40, no. 7, pp. 1937–1952, 2022, doi: 10.1109/JLT.2021.3132863.

[41] M. Rabbani, H. Hosseinianfar, H. Rabbani, H. Brandt-Pearce, "Analysis of Nonlinear Fiber Kerr Effects for Arbitrary Modulation Formats," Journal of Lightwave Technology, vol. 41, no. 1, pp. 96–104, 2023, doi: 10.1109/JLT.2022.3213182.

[42] T. Liu, Z. Xu and T. Jin, C. Xu, T. Tan, M. Zhao, J. Liu, "Analytical Optimization of Wideband Nonlinear Optical Fiber Communication Systems," Optics Express, vol. 30, no. 7, pp. 11345–11359, 2022, doi: 10.1364/oe.453307.

[43] B. Sambo, N. Correia, J. Napoli, A. Pedro, and V. Sambo, N. Correia, B. Napoli, A. Pedro, J. Kiani, L. Castoldi, P. Curri, "Network Upgrade Exploiting Multi Band: S- Or E-Band?" Journal of Optical Communications and Networking, vol. 14, no. 9, pp. 749–656, 2022, doi: 10.1364/jocn.464386.

[44] C. Song, Y. Fan, Q. Lu and A. P. T. Wang, D. Lau, "Efficient Three-Step Amplifier Configuration Algorithm for Dynamic C+L-Band Links in Presence of Stimulated Raman Scattering," Journal of Lightwave Technology, vol. 41, no. 5, pp. 1445–1453, 2023, doi: 10.1109/JLT.2022.3223919.

[45] B. Sambo, N. Correia, J. Napoli, A. Pedro, and V. Castoldi, P. Curri, "Transport Network Upgrade exploiting Multi-Band Systems: S-versus E-band," in 2022 Optical Fiber Communications Conference and Exhibition, OFC 2022 - Proceedings, 2022, pp. 1–3. doi: 10.1364/ofc.2022.w3f.8.

[46] K. Okamoto, S. Minoguchi and Y. Hamaoka, F. Horikoshi, K. Matsushita, A. Nakamura, M. Yamazaki, E. Kisaka, "A Study on the Effect of Ultra-Wide Band WDM on Optical Transmission Systems," Journal of Lightwave Technology, vol. 38, no. 5, pp. 1061–1070, 2020, doi: 10.1109/JLT.2019.2962178.

[47] S. Ivanov, V. V. Sterlingov, P. M. Mishra, S. K. Downie, J. D. Makovejs, "Effective Area Tilt Impact In S+C+L Band Long-Haul Fiber Optic Transmission Systems," in 2022 Optical Fiber Communications Conference and Exhibition, OFC 2022 - Proceedings, 2022, pp. 3–5. doi: 10.1364/ofc.2022.w3e.4.

[48] A. Ghazisaeidi, A. Arnould, M. Ionescu, V. Aref , H. Mardoyan, S. Etienne, M. Duval, C. Bastide, H. Bissessur, and J. Renaudier, "99.35 Tb/s Ultra-wideband Unrepeated Transmission Over 257 km Using Semiconductor Optical Amplifiers and Distributed Raman Amplification," Journal of Lightwave Technology, vol. 40, no. 21, pp. 7014–7019, 2022, doi: 10.1109/JLT.2022.3198518.

[49] W. Hazarika, P. Tan, M. Donodin, A. Noor, S. Phillips, I. Harper, P. Stone, J. S. Li, M. J. Forysiak, "E-, S-, C- And L-Band Coherent Transmission with A Multistage Discrete Raman Amplifier," Optics Express, vol. 30, no. 24, pp. 43118–43125, 2022, doi: 10.1364/oe.474327.

[50] H. Zafar, K Enneth, L K Ereira, M Auro F P,Asras, M Ahmoud R, Hamim, Njum, D Alaver H A., "Compact Broadband (O, E, S, C, L & U Ban Ds) Silicon TE-Pass Polarizer Based on Ridge Waveguide Adiabatic S-Bends," Optics Express, vol. 30, no. 6, pp. 10087–10095, 2022, doi: 10.1364/oe.452823.